Spectroscopic properties of alkali borate glasses containing Cu2+

Georges Calas, Natan Capobianco, Laurence Galoisy

▶ **To cite this version:**

Georges Calas, Natan Capobianco, Laurence Galoisy. Spectroscopic properties of alkali borate glasses containing Cu2+. Journal of Non-Crystalline Solids, 2022, 591, pp.121711. 10.1016/j.jnoncrysol.2022.121711 . hal-03941960

HAL Id: hal-03941960
https://hal.science/hal-03941960

Submitted on 22 Jul 2024

HAL is a multi-disciplinary open access archive for the deposit and dissemination of scientific research documents, whether they are published or not. The documents may come from teaching and research institutions in France or abroad, or from public or private research centers.

L'archive ouverte pluridisciplinaire **HAL**, est destinée au dépôt et à la diffusion de documents scientifiques de niveau recherche, publiés ou non, émanant des établissements d'enseignement et de recherche français ou étrangers, des laboratoires publics ou privés.

Distributed under a Creative Commons Attribution - NonCommercial 4.0 International License

Version of Record: https://www.sciencedirect.com/science/article/pii/S0022309322003106
Manuscript_95fb9bc729d5542e8dc0a9c947f0045f

Spectroscopic properties of alkali borate glasses containing Cu^{2+}

Georges Calas, Natan Capobianco, Laurence Galoisy

Sorbonne Université, CNRS, Muséum National d'Histoire Naturelle, IRD, Institut de Minéralogie, de Physique des Matériaux et de Cosmochimie (IMPMC), 75005 Paris, France

**Corresponding author: georges.calas@sorbonne-universite.fr (G. Calas).*

Abstract

Binary alkali borate glasses R_2O-B_2O_3 (R = Li, Na or K) are a model system for oxide glasses due to the major modification of their structure and properties with alkali concentration. The present study correlates optical absorption and electron paramagnetic resonance (EPR) spectroscopy data on binary alkali borate glasses containing Cu^{2+} in the range 10-33 mol%. These glasses show a color change from light cyan to sky blue with increasing alkali content. The chemical dependence of the spectroscopic properties of Cu^{2+} in alkali borate glasses is different from what is observed for other divalent transition metal ions (Ni^{2+}, Co^{2+}): (i) there is no change in the coordination of Cu^{2+} as a function of alkali content, confirming that tetrahedral Cu^{2+} is rather rare in oxide materials; (ii) as a consequence, the color change of Cu^{2+}-containing glasses as a function of their chemical composition remains limited; (iii) cation field strength does not significantly influence the spectroscopic properties of Cu^{2+}, the alkali content being the main chemical parameter governing Cu^{2+} speciation in these glasses; (iv) there is no clustering of Cu^{2+} ions in low-alkali borate glasses. By correlating the data obtained from optical absorption spectroscopy and from EPR, information is gained on the variation of Cu site geometry as a function of the alkali content of the glass. In low-alkali glasses, the Cu^{2+} sites show a higher distortion than in high-alkali glasses and their coordination geometry is less distributed. This may indicate a link with the rigid superstructural borate units of these glasses. The spectroscopic parameters of Cu^{2+} in low-alkali glasses show also a noteworthy similarity with those of aqueous Cu^{2+} complexes. The smaller site distortion in high-alkali glasses is accompanied by a more covalent character of the π Cu^{2+}-O bonds, resulting from a weakening of the B-O bonds due to the progressive conversion of $^{[3]}B$ to $^{[4]}B$ with increasing alkali content. The color changes from light cyan to sky blue due to the increase in absorption efficiency in the red portion of the visible spectrum. Indeed, in high-alkali glasses, a greater distribution of the Cu^{2+} sites causes a broadening of the Cu^{2+} absorption band. These modifications are explained by considering the influence of axial ligands on the distortion of Cu^{2+} sites. The intensity of this axial distortion governs the anisotropy of the Cu^{2+} sites, even if the contribution of axial ligands to the local charge balance of Cu^{2+} remains minor. The Cu^{2+} speciation in alkali borate glasses derived from this spectroscopic approach is consistent with a bond-valence model. As Cu^{2+} is used widely as a structural probe in crystals and glasses, such a bond-valence approach may shed light on the local environment of Cu^{2+} in oxide glasses.

© 2022 published by Elsevier. This manuscript is made available under the CC BY NC user license
https://creativecommons.org/licenses/by-nc/4.0/

Keywords: borate glasses; Cu^{2+} spectroscopy; glass structure; UV-visible spectra; Electron Paramagnetic Resonance (EPR); crystalline borates.

1. Introduction

By contrast to most glasses, which are considered to have only a short range ordered structure, borate glasses show some medium range order due to the presence of rigid superstructural units [1], based on an arrangement of 3- and 4-coordinated boron (referred hereafter to as $^{[3]}$B and $^{[4]}$B, respectively). Up to a Na_2O/B_2O_3 ratio of about 0.5, B-coordination in oxide melts and glasses varies with composition, temperature and pressure. The coexistence of $^{[3]}$B and $^{[4]}$B causes borate glasses to exhibit unique structure-property relationships, because of the complex interplay between these two B coordination states and the other glass components. This medium range order in binary alkali borate glasses varies with the alkali content [2]. The boron coordination change from $^{[3]}$B to $^{[4]}$B with increasing alkali content modifies the local structure of the glasses, as the alkali ions associated to B turn from a modifying to a charge-compensating role. As a consequence, alkali borate glasses exhibit important modifications of their physical and chemical properties as a function of cation content and cation field strength [3].

When containing transition metal ions, binary alkali borate and borosilicate glasses exhibit a spectacular color change as a function of the alkali nature and content, which has been mostly approached in the past through optical absorption spectroscopy [4,5]. X-ray absorption spectroscopy (XAS) has provided structural scenarios explaining such color changes, e.g. in Ni- and Co-containing alkali borate glasses, in which these elements exist only in the divalent state. The correlation between optical absorption spectroscopy and XAS has shown the importance of 5-coordination of Ni^{2+} in oxide glasses [6,7]. The color due to Ni^{2+} in alkali borate glasses varies from green in 10 mol% R_2O to glasses to brown at higher alkali content and even deep purple at high K_2O content, due to the progressive conversion of Ni^{2+} from 6- to 5- and 4-fold coordination [7,8]. This sensitivity to the concentration and field strength of the alkali explains the large palette of colors of Ni-containing alkali borate glasses. Later studies have shown that the geometry of the Co^{2+} site shows a similar chemical dependence in the same borate glass compositions: there is a decrease in the coordination number of Co^{2+} from 6 to 5 and 4 with increasing alkali levels and decreasing field strength of the alkali. This causes the color to vary from pink to blue in 10% R_2O and 30% R_2O glasses, respectively, due to the conversion of Co^{2+} from 6- to 5- and 4-fold coordination [9]. Here too, decreasing the alkali field strength (from Li^+ to K^+) enhances the formation of low coordinated sites. Similarly to *3d* elements, the coordination number of uranyl groups in borate glasses decreases with increasing glass alkalinity, as shown by the smaller number of equatorial ligands measured by X-ray Absorption Near Edge Structure (XANES) [10].

It is interesting to investigate the behavior of other divalent transition metal ions in alkali borate glasses, as a function of the alkali content or of the alkali field strength. Copper may exist in glasses under oxidation states usually ranging between 0 and +2 [4,5] and Cu^{2+}, a d^9 ion causes the well-known blue to green color of glasses and crystals [4]. By contrast, Cu^0 metallic nanoparticles cause an intense red coloration [4] and Cu^+ does not give rise to any glass coloration, as it is a d^{10} ion [11]. As Cu^{2+} has only one half-filled electronic orbital, this $3d^9$ configuration gives rise to a relatively simple energy level structure with one ground state ^2E_g and one excited state $^2T_{2g}$ in regular octahedral fields [11]. Divalent copper spectroscopy has been extensively investigated in glasses since the pioneering studies of Hosono and coworkers [12-14]. The colors caused by Cu^{2+} in glasses vary between blue and cyan, as in stained glasses [15,16] or antique tesserae [17]. Variations in the intensity of the crystal field are not the only reason for this change of color. Octahedral Cu^{2+} ions undergo a Jahn-Teller distortion that also affects glass color. Cu^{2+} ions constitute a useful spectroscopic probe of the local structure of glasses [12,13]. In addition, recent studies on Na borate glasses show an original sensitivity of Cu^{2+} spectroscopy to the influence of other doping impurities in borate glasses [14,18].

Numerical modeling [19,20] shows an elongation by 3 to 16% of the axial Cu-O bonds, as a result of a Jahn Teller effect, a value close to the 10% axial elongation of the Cu^{2+} site substituted in crystalline lithium borates [21]. In glasses, the focus has been mostly on specific borate glasses within a limited range of alkalis, therefore leaving aside questions regarding the differences between low- (< 20 mol% alkalis) and high-alkali glasses [12,13,22]. The origin of these differences still raises questions. As EPR provides evidence of a modification of the Cu^{2+} sites between low- and high-borate glasses, XAS does not evidence any sharp change, though the presence of Cu^+ may limit an accurate use of this technique [23]. Moreover, optical absorption data are still scarce, especially in the near infrared. In this work, we determine the relation between EPR and optical absorption spectroscopy data in binary Li-, Na- and K-borate glasses, by considering the influence of the alkali concentration, in the range 10-33 mol% alkali oxides, and of the alkali field strength. This structural information is compared to the surrounding of Cu^{2+} in crystalline borates and with structural scenarios expected from from a bond-valence modeling. These data show that Cu^{2+} occurs in axially elongated octahedra, the position of the axial ligands being dependent on the links between the Cu-sites and the borate framework. The absence of a clear coordination change of Cu^{2+} in alkali borate glasses limits a strong variation of the color with glass composition and is a major difference with what is observed for Co^{2+} and Ni^{2+}, due to the different electronic properties of these ions.

2. Experimental methods

We synthesized, by a melt quenching technique, binary alkali borate glasses, $nX_2O - (1\text{-}n)\ B_2O_3$, where X is Li, Na or K and n ranges from 0.1 to 0.33. Each batch of 3g consisted of reagent grade CuO, alkali carbonate (Li_2CO_3, Na_2CO_3, K_2CO_3) and H_3BO_3. The raw materials were dehydrated overnight, at temperatures ranging from 150°C to 350°C and mixed together in an agate mortar. The resulting powder was then melted in a platinum crucible under ambient atmosphere at 1100°C for 2 h. The glass was reground and re-melted for 2 h at 1100 ° C. It was then cast between two copper plates, annealed for 2 h at 20°C below the glass transition temperature of each glass and stored in paraffin oil to prevent hydration. The X-ray amorphous nature of the glasses was checked by X-ray diffraction (**Fig. S1**). Glass plates were shaped for EPR spectroscopy. **Table 1** summarizes the composition of the samples synthesized.

Table 1. Nominal composition of the alkali borate glasses investigated (mol%). The samples were added 0.2 mol% CuO for each batch.

	B_2O_3	Li_2O	Na_2O	K_2O
LiB10	90	10		
LiB14	86	14		
LiB21	80	21		
LiB25	75	25		
LiB33	67	33		
NaB10	90		10	
NaB14	86		14	
NaB25	75		25	
NaB33	67		33	
KB10	90			10
KB14	86			14
KB25	75			25
KB33	67			33

Optical absorption spectroscopy analyses were performed on glass sections mechanically polished on both sides. The thickness of the polished slabs was determined by an Olympus ultrasound gauge 45MG-X-MT-E. Optical absorption spectra were recorded at room temperature using a Perkin-Elmer Lambda 1050 UV–Visible-NIR spectrophotometer in transmission mode in the range of 300–3300 nm (33330–3030 cm^{-1}). The absorption spectra, corrected from reflection at the glass surface, were normalized to sample thickness.

For Electron Paramagnetic Resonance (EPR) measurements, the glasses were shaped as cylinders for a measure in silica (Suprasil) tubes for X-band. The EPR signals were collected using a Bruker ESP 300 at X-band (9.5 GHz), with a field modulation of 100 kHz and an amplitude modulation of 1 mT. The measurements were performed at different microwave powers to avoid signal saturation. The inter-comparison of the X-band EPR signals was achieved by normalization to the mass of the sample, the gain, the amplitude modulation and the square root of power (expressed in mW). The same volume of sample, accurately weighted, was used for each spectral measurement to minimize inaccuracies due to the variation in the sample position within the EPR cavity.

3. Results

3.1. Optical absorption spectroscopy

The glasses present different colors in terms of hue and saturation (**Fig. 1**), ranging from light cyan to sky blue with increasing alkali content. In addition to hue variations, the saturation of the coloration is larger in alkali rich glasses. This may be related to the chemical dependence of the Cu^{2+} site geometry and of the redox ratio Cu^{2+}/Cu_{total}. The color change of these glasses occurs near 20 mol%, a value similar to the color change observed in binary alkali borate glasses doped with other transition elements, as above mentioned.

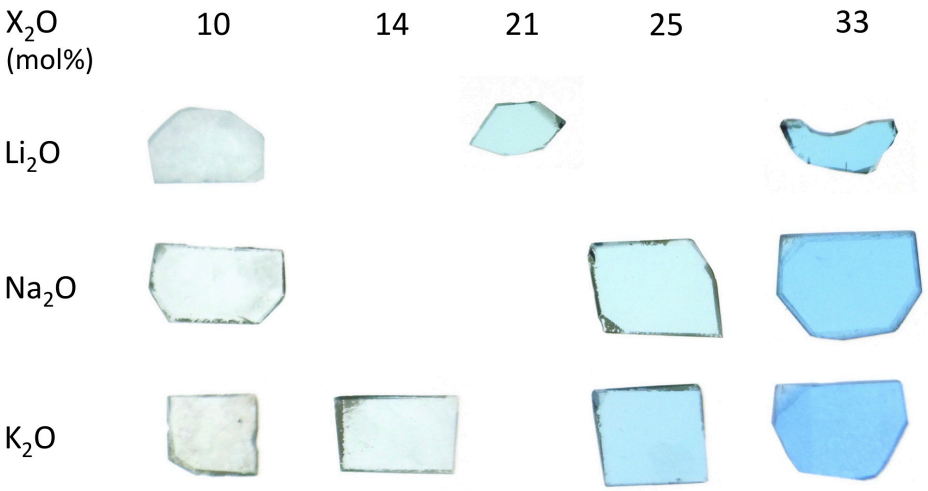

Fig. 1. Color of the investigated glasses

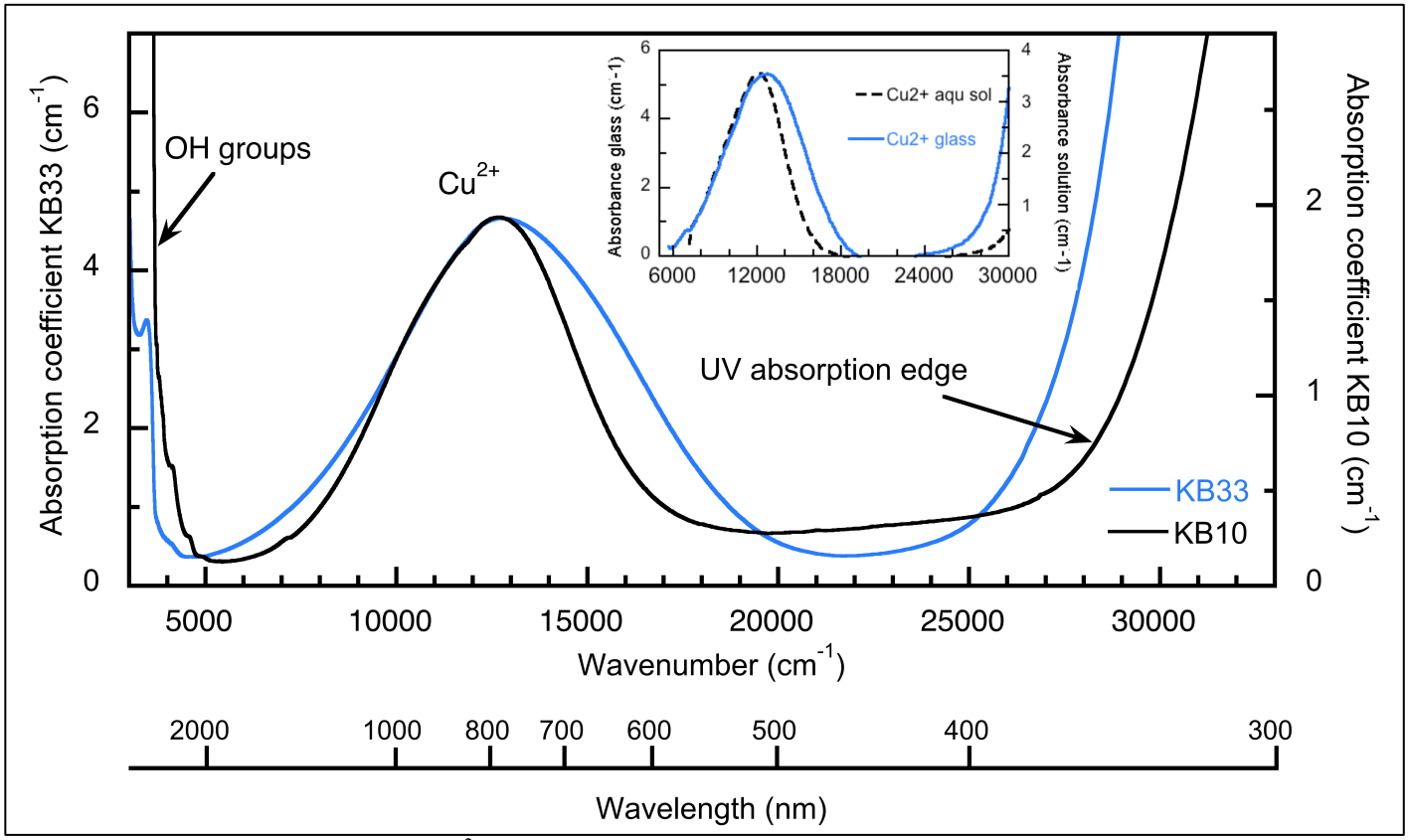

Fig. 2. Optical absorption spectra of Cu^{2+} in two potassium borate glasses. The spectra have been normalized to the same intensity of the Cu^{2+} absorption band, due to a higher absorbance at higher alkali content. The inset compares the Cu^{2+} absorption spectra in a Na-silicate glass and in aqueous solution (data after [24], modified), showing a similar trend. The spectra have been normalized to the same intensity of the Cu^{2+} absorption band for comparison purpose.

The optical absorption spectra of low- and high K-borate glasses show several differences (**Fig. 2**). Three spectral domains are recognized. (i) In the near infrared, an intense absorption near 3500 cm^{-1} arises from the stretching vibrations of hydroxyl impurities. This absorption of OH groups is more important in low alkali than in high alkali glasses. On the low wavenumber side, it is superimposed to an abruptly rising absorption due to the vibrations of the borate network, such as the first overtone of the $^{[3]}$B-O stretching vibration near 2800 cm^{-1}; ii) In the visible part of the spectrum, the large and asymmetrical Cu^{2+} absorption band is centered near 12500-13000 cm^{-1}. This band is narrower by about 20% and less intense by 40% in the alkali-poor KB10 glass than in the alkali-rich KB33 glass. A similar difference is observed between an aqua-complex and a silicate glass (**Fig. 2, Inset**), which may arise from the disorder-induced distribution of the geometry of the Cu^{2+} sites in glasses by opposition to aqueous solutions; (iii) In the near UV, the position of the absorption threshold depends also on glass composition. It shifts to lower wavenumbers in alkali-rich compositions. As the intensity of the Cu^{2+} absorption band also increases in alkali-rich glasses, the modification of the UV threshold can be linked to an $O^{2-} \longrightarrow Cu^{2+}$ charge transfer, though an intervalence charge transfer $Cu^{+} \longrightarrow Cu^{2+}$ may be another possibility, as suspected in other borate glasses [25]. The influence of an intraconfigurational $3d^{10}4s^{0} \longrightarrow 3d^{9}4p^{1}$ transition of Cu^{+} can be discarded as this transition occurs at wavenumbers above 35000 cm^{-1} and is not easily detected in glasses [26].

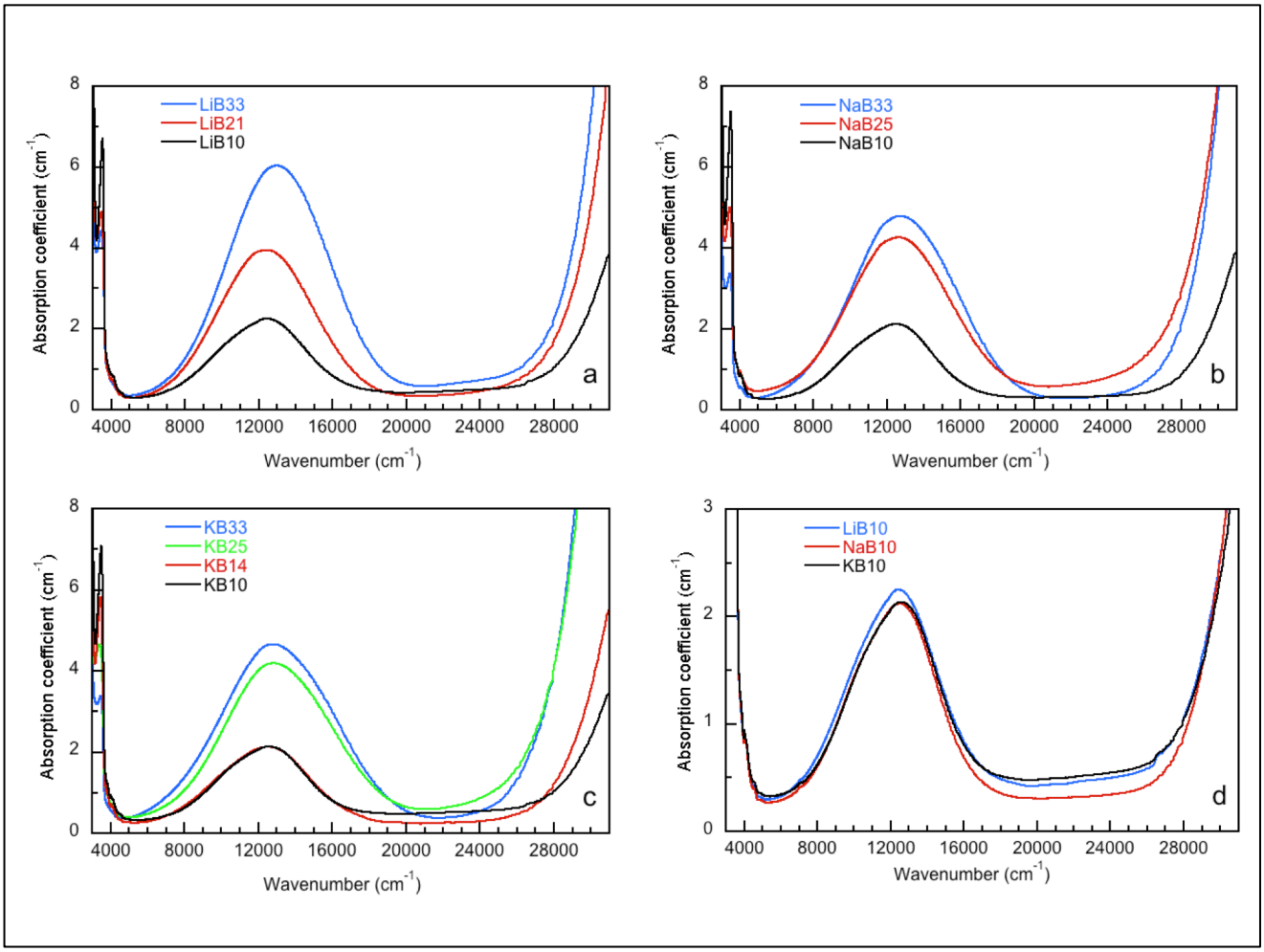

159

160 **Fig. 3.** Optical absorption spectra of binary alkali borate glasses for alkali R levels varying between 10 and 33 mol%
161 R_2O. (a): Li-borate glasses; (b): Na-borate glasses; (c): K-borate glasses. These spectra show similar differences
162 between alkali-poor and alkali-rich glasses for the three spectral domains discussed in the text: OH stretching modes,
163 Cu^{2+} crystal field band and UV-threshold. (d): Alkali-poor borate glasses show similar Cu^{2+} absorption band and
164 possess the same transmission window, which give them a color independent of the nature of the alkali.

165

166

167 **Fig. 3** depicts the optical absorption spectra, after normalization to a linear absorbance scale. All spectra exhibit
168 the broad Cu^{2+} absorption band centered near 12500-13000 cm^{-1}, close to the boundary between the visible range and
169 the near infrared. Its high-energy side absorbs red radiations, defining a characteristic transmission window in the blue-
170 green domain. The position and shape of this band vary with glass composition. In alkali-poor glasses, it is of low
171 intensity and asymmetrical on its low wavenumber side with a shoulder near 10000 cm^{-1}. We find a good agreement

between the position and width of the Cu^{2+} absorption band in these low alkali glasses and the data obtained in aqueous solutions, where Cu^{2+} occurs as hexa-aquo complexes [24,27]. At higher alkali content, the intensity and width of this band increase and an asymmetry appears on its high wavenumber side, due to a shoulder near 14 000 cm^{-1}. The concentration and, to a lesser extent, the nature of the alkali influence the shape of the absorption band, as exemplified in **Figs 3a, 3b and 3c**, with the exception of the alkali poor glasses, for which the Cu^{2+} band is almost identical for the three Li, Na and K three XB9 glasses (**Fig. 3d)**.

The position of the Cu^{2+} absorption band shifts only by less than 5% over the glass composition range investigated (**Fig. S2**). The influence of the alkali content of borate glasses on the color imparted by Cu^{2+} is more limited than for other transition metal ions as Ni^{2+} [8] or Co^{2+} [9] that suffer major coordination changes in alkali borate glasses, from 6-, to 5- and 4-coordination at increasing alkali content. The small modifications observed in the optical spectra indicate the absence of such drastic coordination change of Cu^{2+} in this composition range. However, by contrast to the position of the band, its width increases by about 30% with the alkali content (**Fig. 4**) causing a perceptible color change (see **4.2**).

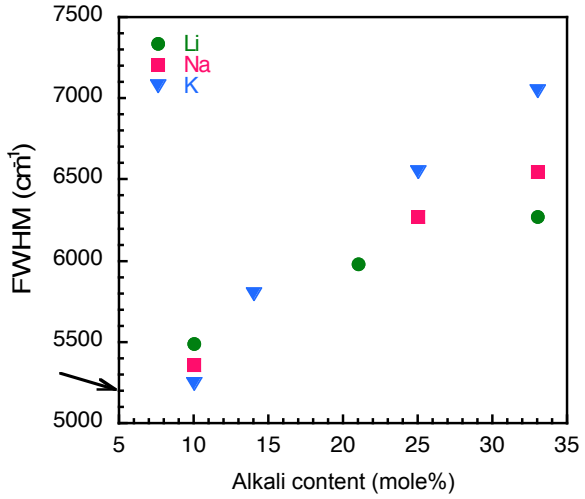

Fig. 4. Full width at half maximum of the Cu^{2+} band. The arrow indicates the value observed for the Cu^{2+} aqua ion [27], which is similar to the values observed in low alkali borate glasses.

3.2 EPR spectroscopy

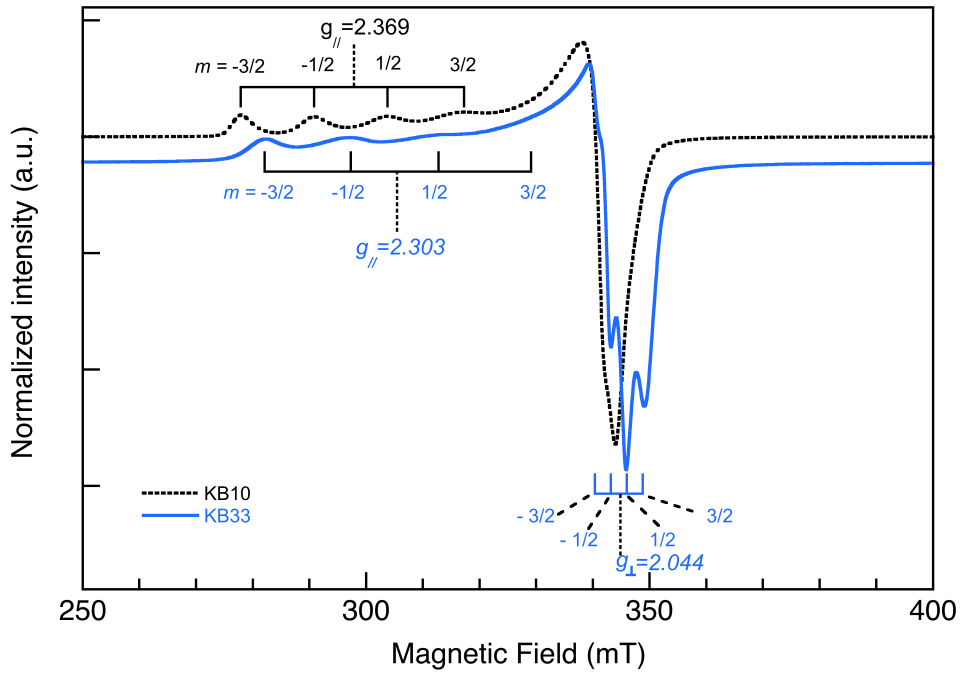

Fig. 5. EPR spectrum of Cu^{2+} in the KB33 and KB10 glasses. $g_{//}$ and $g_{\perp}$ are the parallel and perpendicular components of the *g*-factor, respectively. The parallel signals are on the low field side of the spectrum, an indication of the elongation of the Cu^{2+} site. The parallel and perpendicular components of the hyperfine *A*-tensor, $A_{//}$ and $A_{\perp}$, respectively, are designated by the interaction with the nuclear spin (varying from -3/2 to +3/2). The *g*-factor is defined by the relation $h\nu=g\beta H$, where ν is the microwave frequency, H is the applied magnetic field, β is the Bohr magneton, and h is the Planck constant. It is determined from the center of each hyperfine structure and its value is given for the two parallel structures of KB33 and KB10 glasses and for the perpendicular structure of KB33, which is resolved due to the large value of the hyperfine structure in high alkali glasses.

The EPR data do not reveal the presence of Cu^{2+}-rich clusters. The baseline is horizontal, indicating the absence of superparamagnetic contributions that would arise from Cu^{2+}-rich clusters. Indeed, the presence of these clusters would be characterized by a broad and asymmetric signal, as observed in presence of copper oxide clusters and nanoparticles [28]. An abundant literature has been published on the EPR spectra of diluted Cu^{2+} in borate glasses [12-14,18-20,22,25,29-31]. The spectra of the KB10 and KB33 glasses (**Fig. 5**) show two sets of well-resolved, equally spaced hyperfine components, characterizing the asymmetrical Cu^{2+} site. The parallel hyperfine structure occurs at a

lower magnetic field than the perpendicular structure indicating $g_{//} > g_{\perp} > 2.0023$ (g_e): this corresponds to an axial elongation of the octahedral Cu^{2+}-site along the z-axis, with a ground state being the d_x^2-$_y^2$ orbital ($^2B_{1g}$ state). The EPR signals occur at a lower magnetic field in the low alkali glass KB10 than in the high alkali glass KB33, indicating larger *g*-values in the former relative to the latter. As it will be discussed in **§4.1**, this spectral shift corresponds to larger Cu_{axial}-O bond lengths. This is in contrast to the clustering observed for other divalent transition metal ions (Ni^{2+}, Co^{2+}) and Zn^{2+} in low-alkali borate glasses [32,33].

The position of the hyperfine components (**Fig. 5**) is characteristic of an axial Cu^{2+} signal. The perpendicular structure is narrower and less resolved in low-alkali than in high alkali glasses because of a smaller hyperfine splitting that causes the four hyperfine components to overlap. The parallel hyperfine structure shows a larger hyperfine splitting arising from the elongation of the Cu^{2+} site. It shows also a progressive inhomogeneous broadening and weakening with increasing magnetic field. The same behavior has been observed on the EPR spectra of Cu^{2+} in silicate glasses and aqueous solutions, the former being more disordered than the latter [34]. The spectra are better resolved in alkali-poor glasses, as previously observed for the optical properties (see **3.3**). This indicates a more limited local disorder as compared to alkali-rich compositions, probably linked to the presence of $^{[3]}$B-containing super-structural units(see **4.2**).

4. Discussion

4.1 Structural information from EPR

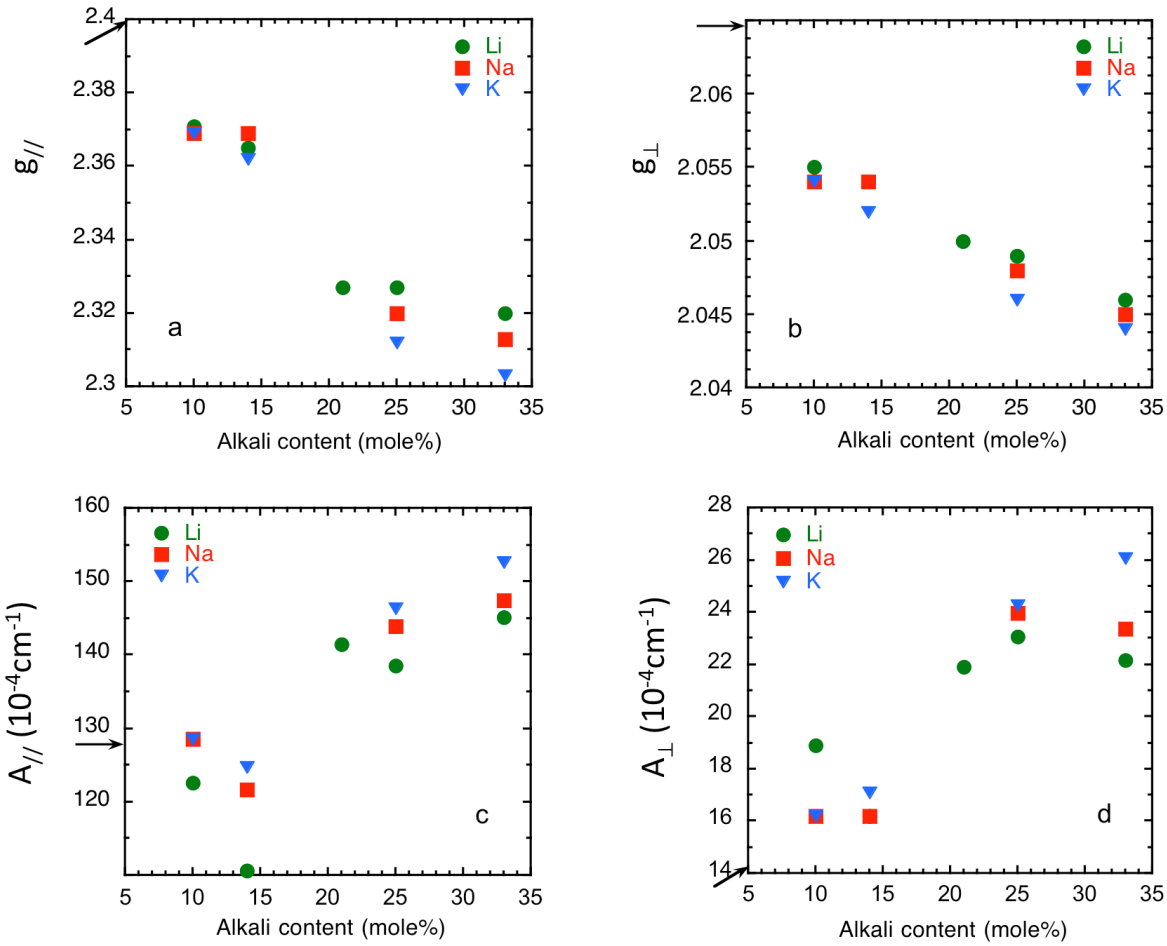

Fig. 6. Evolution of the EPR parameters as a function of the nature and concentration of the alkali. (a) and (b) represent the variation of the parallel and perpendicular *g*-factor, respectively; (c) and (d) represent the variation of the parallel and perpendicular hyperfine parameters, respectively. The arrow symbols indicate the values obtained for the EPR parameters (parallel components) of the Cu^{2+} hexa-aqua complex in D_{2h} symmetry [data from 35,36].

Previous studies demonstrated that EPR parameters of Cu^{2+} show a marked chemical dependence in binary alkali borate glasses [12,13,22,37]. This dependence is similar for the parallel and perpendicular components (**Fig. 6** and **Table S1)**. However, as the *g*-factor decreases with increasing alkali content, the hyperfine coupling constant *A* follows an inverse trend. It results a noteworthy inverse linear relationship between $g_{//}$ and $A_{//}$ as a function of glass composition (**Fig. 7a**). A similar relationship has been observed in most glassy systems containing Cu^{2+} [37,38]. The seminal work of Peisach and Blumberg [39] established experimentally the general linear trend anti-correlating $g_{//}$ and

241 $A_{//}$ values in Cu^{2+} complexes. This inverse relation has been modeled by DFT calculations on Cu^{2+} complexes with
242 oxygen ligands [40]. If we assume a similar behavior of the EPR parameters of Cu^{2+} in glasses and in solutions,
243 decreasing $g_{//}$ while increasing $A_{//}$ values at higher alkali content corresponds to shorter Cu-$O_{equatorial}$ bond lengths. Such
244 a shortening increases the sharing of *d*-electron density between Cu^{2+} and its oxygen neighbors, i.e. a larger
245 delocalization of Cu^{2+} *d*-electron density [40,41]. By contrast, large bond lengths enhance the localization of the *d*-
246 electron density on Cu^{2+} in alkali-poor borate glasses. It is of interest that the EPR parameters of these alkali-poor
247 glasses are close to those found in aqua-complexes, as based on experiment [35] and DFT modeling [36]. This
248 similarity between Cu^{2+} EPR parameters in alkali-poor borate glasses and in solutions is illustrated in **Figs 6** and **7**.
249

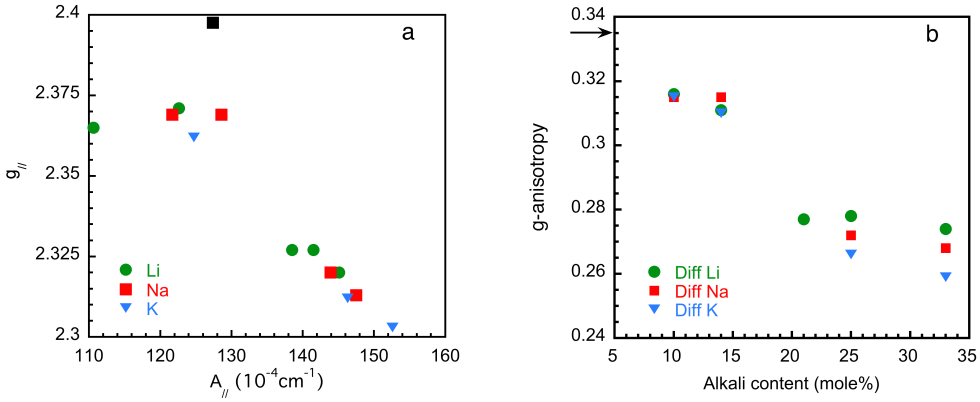

250 **Fig. 7**. (a): Correlation between the EPR parameters $g_{//}$ and $A_{//}$ in alkali borate glasses. The black square represents the
251 value for Cu^{2+} aqua complexes using the data from [35,36]. (b): Evolution of the anisotropy of the *g*-factor, as
252 expressed by $\Delta g = g_{//} - g_{\perp}$.

253

254

255 The anisotropy of the *g*-factor, obtained from the difference between the parallel and the perpendicular *g*-factor
256 components, characterizes the magnitude of the Cu^{2+} site distortion. This anisotropy decreases with increasing alkali
257 content, indicating a smaller site distortion as compared to low alkali borate glasses (**Fig. 7b**).

258

259 ***4.2 Optical properties of Cu^{2+} and the cyan to blue color change of borate glasses containing Cu^{2+}***

260 The molar extinction coefficient ε of Cu^{2+} increases with the alkali content of alkali borate glasses,

approximately doubling from 25 to 50 $L.mol^{-1}.cm^{-1}$ in the 11-33 mol% Na_2O range [5]. The 50 $L.mol^{-1}.cm^{-1}$ value is consistent with that determined in similar air-melted Na_2O-$3B_2O_3$ glasses by Duran and Navarro [42]. As the in-plane π-bonding parameter increases also at high alkali content (see **4.5**), covalency effects may play a role in this evolution of ε values.

The differences between low- and high-alkali borate glasses evidenced by EPR correspond also to a modification of the optical absorption properties of Cu^{2+}, causing a color change easily detected by the naked eye (**Fig. 1**). It is characterized by a broadening of the Cu^{2+} absorption band and by a modification of its shape at high alkali content. This causes the transmission window to narrow around the blue region of the spectrum, giving rise to the color change visually observed. The absorption band may broaden because of a larger distribution of Cu-O bond lengths or from a modification of the intensity of the quadratic distortion of the Cu^{2+} site. As the EXAFS data obtained on Cu-containing alkali borate glasses show only a limited radial disorder of the Cu-O bonds [23], an O-Cu-O bond angle distribution may be at the origin of this broadening.

After subtracting a linear baseline, the Cu^{2+} absorption band has been fitted with Gaussian components. The deconvolution is considered satisfactory when the residue is less than 1% of the source value at all points and the result remains stationary for different starting configurations tested. A Gaussian lineshape is expected for crystal field transitions scaled in wavenumbers [11,43] as it is a scaling proportional to energy. Only a few studies present Cu^{2+} optical absorption spectra inadvertently Gaussian fitted on the basis of a wavelength scale [44]. A three-Gaussian modeling gives consistent results for all samples (**Fig. 8a**). It corresponds to the three electronic transitions expected from the analysis of the electron level diagram in D_{4h} site symmetry (see **4.2**).

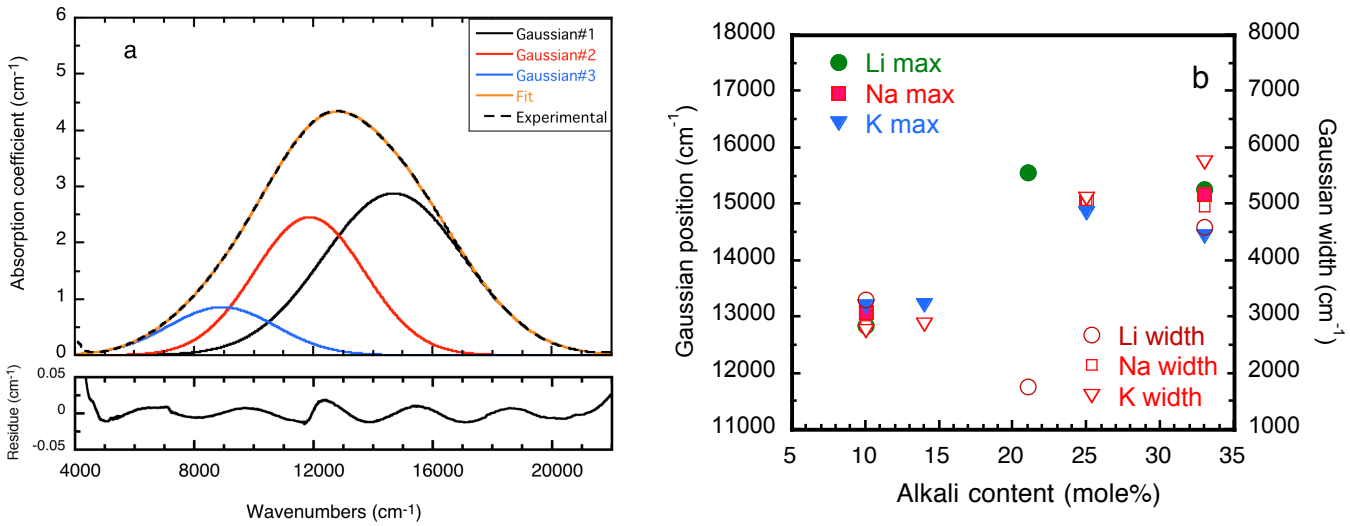

Fig. 8. (a): Fitting of the main Cu^{2+} band into 3 Gaussian components for the optical absorption spectrum of the KB33 sample. These three components are assigned to the three transitions expected in a distorted quadratic symmetry, as indicated on **Fig. 10**. The residual of the fit is shown at the bottom. (b): Position of the maximum absorbance and full width at half maximum (FWHM) of the ν_1 Gaussian component. As the high wavenumber side of this band absorbs in the red-orange region of the spectrum (up to 20000 cm^{-1}), a shift in its position will modify the glass color.

For most glasses, the nature of the alkali has a limited influence on the energy of the electronic transitions. This is especially true for alkali-poor glasses, which present an almost identical absorption band, independently of the field strength of the alkali (**Fig. 3d**). By contrast, there is a marked difference between low and medium alkali glasses (**Table S2**). At low alkali levels, the Gaussian components ν_1 and ν_2 are closely located. As component ν_3 is more distant, this causes an asymmetry of the low wavenumber side of the Cu^{2+} absorption band. At higher alkali content, the three components move away from each other. The increasing spacing between components ν_1 and ν_2 is responsible for the broadening of the band (**Fig. 2**). This causes an asymmetry of its high wavenumber side, affecting the transmission window in the visible range and modifying the color of the glass from cyan to blue. Indeed, the maximum spectral sensitivity of the human eye under daylight conditions is at wavenumbers close to 18000 cm^{-1}. This makes the visual evaluation sensitive even to the minor variations of the Cu^{2+} absorption band. Indeed, the O^{2-} to Cu^{2+} charge transfer band in the near UV does not affect the glass color as it absorbs only weakly the short wavelengths of the visible spectrum [26].

In order to emphasize the evolution of the hue with glass composition, the colorimetric coordinates have been calculated by normalizing the absorbance of the Cu^{2+} band to an optical density of 10 (**Fig. 9**). The potassic glasses present the largest variation of color coordinates: as shown on **Fig. 4**, K-rich glasses show the broadest Cu^{2+} band, which absorbs more efficiently the red portion of the visible spectrum than in the other glasses. This results in a higher purity of the blue color.

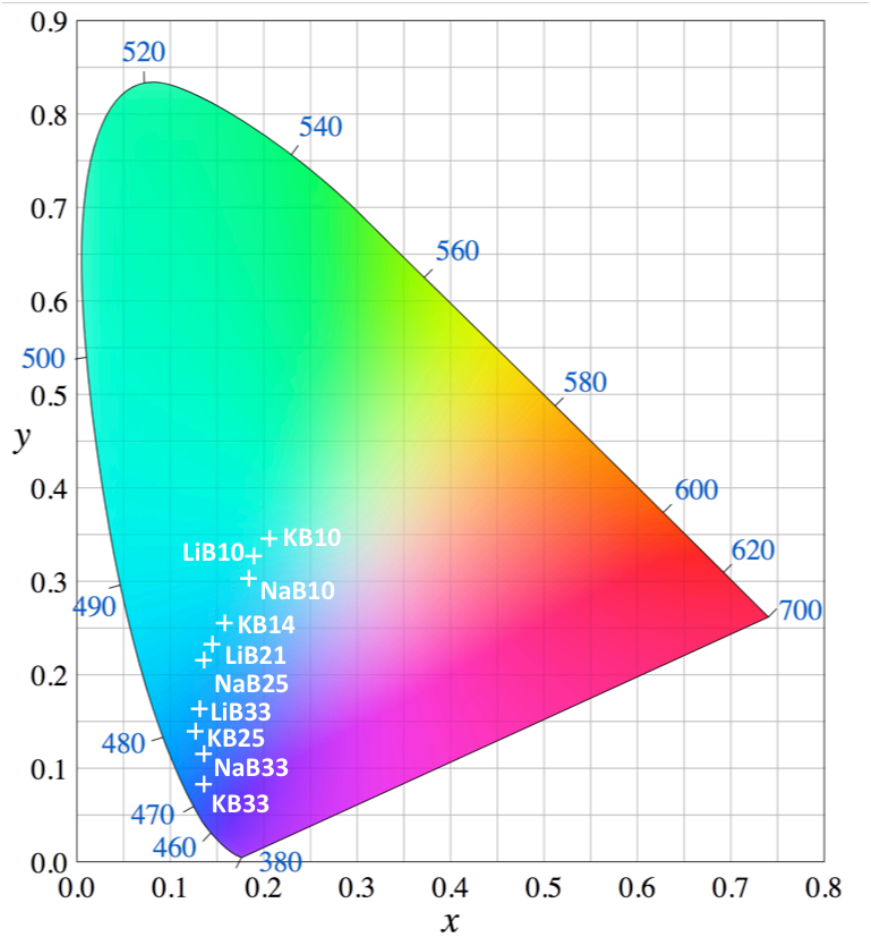

Fig. 9. Colorimetric coordinates of copper-doped alkali borates. The saturation has been overstated to make more explicit the colorimetric differences, as explained in the text. The purity of the color increases in high alkali glasses.

4.3 Chemical dependence of Cu^{2+} crystal field parameters in alkali borate glasses

Cu^{2+} has one unpaired electron, corresponding to the d^9 configuration, extensively investigated in crystalline materials [11,45-47]. In an octahedral crystal field, the free ion term ^2D splits into ground ^2E_g and excited $^2T_{2g}$ levels and only one crystal field parameter, $10Dq$, needs to be considered. As the Jahn-Teller effect lowers site symmetry down to

D_{4h} or lower, three crystal field parameters (*Dq*, *Ds*, *Dt*) are operational and the ^2E_g and $^2T_{2g}$ levels further split into $^2B_{1g}(d_{x^2-y^2})$ and $^2A_{1g}(d_{z^2})$ and into $^2B_{2g}(d_{xy})$ and $^2E_g(d_{xz}, d_{yz})$ levels, respectively. As a consequence, three optical transitions from the ground state ^2E_g, are expected. They will be referred to as ν_1, ν_2 and ν_3. (**Fig. 10**).

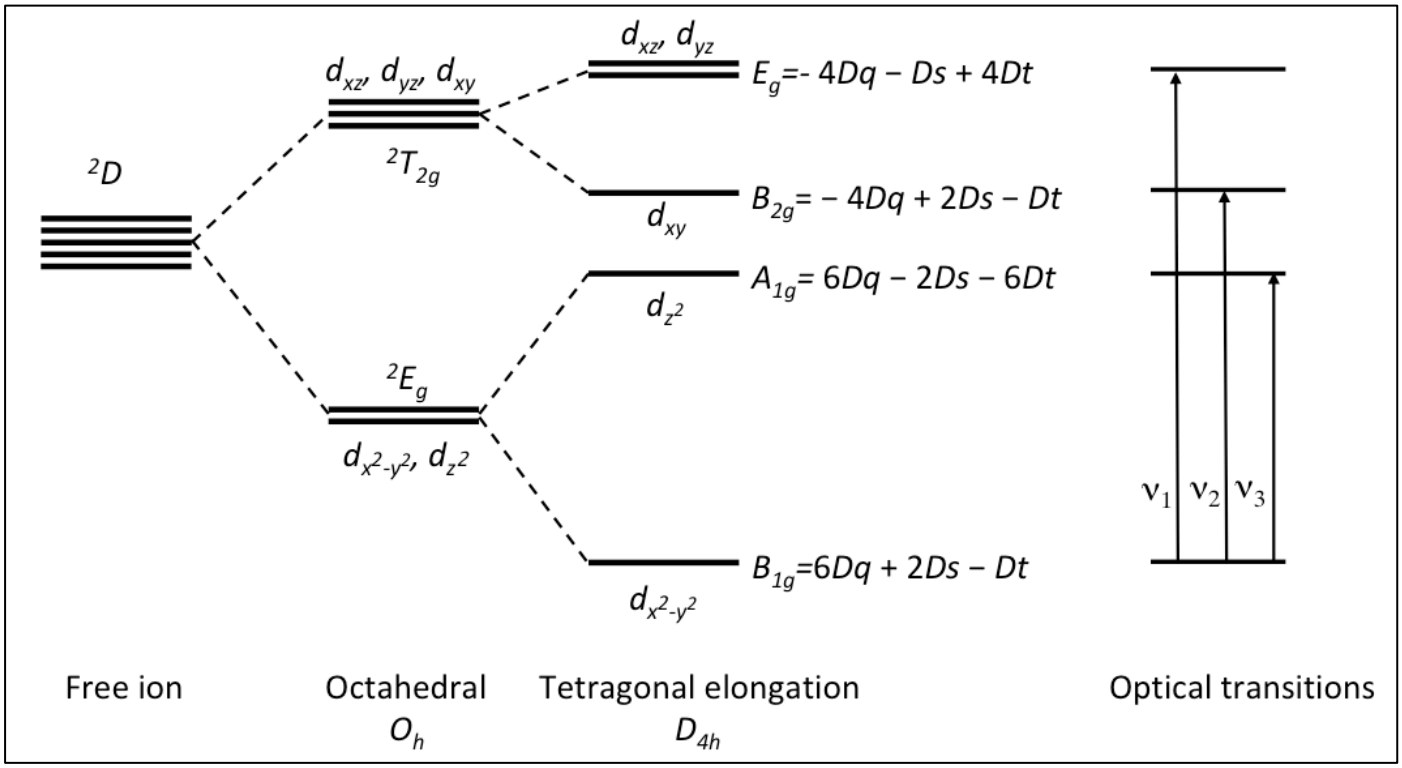

Fig. 10. Schematic representation of the energy levels of the Cu^{2+} ions for tetragonally elongated octahedral coordination. *Dq* is the cubic field parameter and *Dt* and *Dt* are the tetragonal field parameters. The parameterization of the electronic levels is indicated on the right side of each level [after 11 and 43, modified].

The *Dq*, *Ds* and *Dt* parameters define the energy difference between these levels [48]. The matrix elements for the four electronic states of Cu^{2+} in a D_{4h} crystal field are given by the following set of equations:

$$E(^2A_{1g}) = 2+6Dq - 2Ds - 6Dt\ (d_{z^2}) \quad (1)$$

$$E(^2B_{1g}) = 6Dq + 2Ds - Dt\ (d_{x^2-y^2}) \quad (2)$$

$$E(^2E_g) = -4Dq - Ds + Dt\ (d_{xz}, d_{yz}) \quad (3)$$

$$E(^2B_{2g}) = -4Dq + 2\,Ds - Dt\ (d_{xy}) \quad (4)$$

Three *d*-*d* absorption bands are thus expected in tetragonal (D_{4h}) symmetry and the three Gaussian components used to fit the Cu^{2+} absorption band may be assigned to the ν_1, ν_2 and ν_3 transitions of **Fig. 10**, one in the near infrared and two in the red region of the visible spectrum [11,43]. This ordering of the energy levels is consistent with the EPR spectra. Indeed, the relation $g_{//} > g_{\perp} > 2.0023$, observed for most Cu^{2+}-site geometries (elongated octahedral, square pyramidal or square planar) is consistent with a $d_{x^2-y^2}$ ground state.

The axial ligands govern Cu-site anisotropy. Their contribution creates a distorted tetragonal field, which shifts the *d* - *d* electronic transitions to lower energy relative to a square-planar geometry, as was shown by DFT calculations on Cu^{2+} aqua-complexes [36]. However, the $d_{x^2-y^2} \rightarrow d_{xy}$ transition (ν_2 transition) undergoes only a small influence from these axial ligands and remains at about the same value in all alkali borate glasses investigated (**Table S2**). By contrast, the effect of an axial coordination is more pronounced for the $d_{x^2-y^2} \rightarrow d_{z^2}$ transition (ν_3 transition). Indeed, the *d*-orbitals having "*z*" components (d_{xz} , d_{yz} , d_{z^2}) experience an increase in the electrostatic repulsion from axial ligands.

The cubic *Dq* and tetragonal *Ds* and *Dt* crystal field parameters (**Table S3**) can be extracted from the value of the ν_1, ν_2 and ν_3 transitions. The cubic parameter *Dq* has similar values for all glasses, at ca. 1220 cm^{-1}, with only 1% dispersion. This value is consistent with those found in crystalline compounds [11]. The alkali concentration and field strength do not influence *Dq* and there is no chemical trend apparent. The tetragonal parameters show a distinct behavior. The *Ds* parameter values are dispersed by about 20%, without any significant trend but they remain in the same range as in minerals [11]. By contrast, the *Dt* parameter shows an inverse dependence with the alkali content (**Fig. 11a**), showing that Cu^{2+} sites are more distorted in low-alkali than in high-alkali borate glasses. *Dt* parameter values fit well within the range determined in most Cu-crystalline compounds [11,45-47].

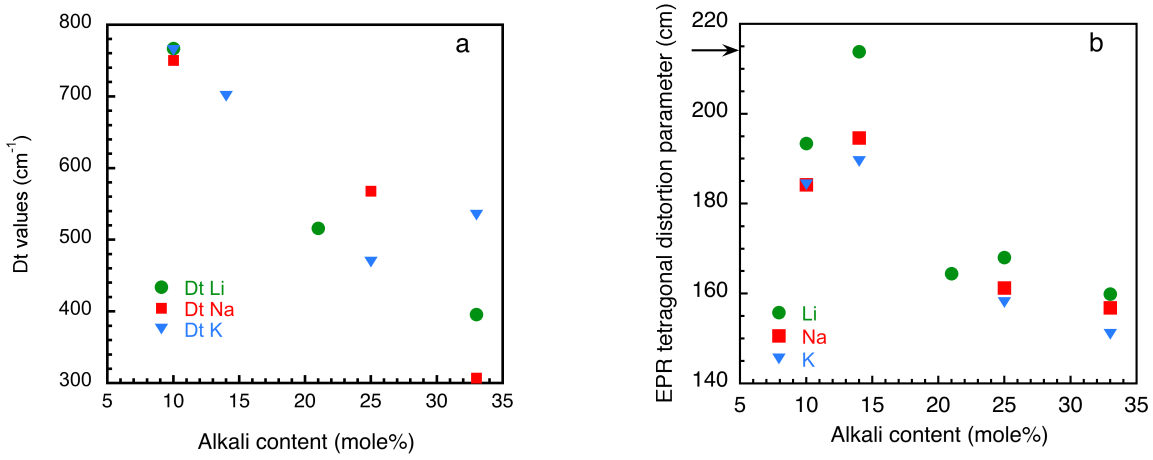

Fig. 11 (a) Evolution of the optically derived tetragonal crystal field parameter *Dt* with glass composition. (b) Evolution of the tetragonal distortion parameter derived from EPR (defined by the $g_{//}/A_{//}$ ratio, in cm values). The arrow symbol represents the value found for Cu^{2+} aqua complexes.

4.4 Cu^{2+} site distortion

The distortion of the Cu-site can be discussed at the light of the data obtained from EPR and optical spectroscopy: anisotropy of the *g*-factor and tetragonal distortion parameter for the former and tetragonal field parameter *Dt* and splitting of the Gaussian components of the Cu^{2+} absorption band for the latter. **Figs 11a** and **11b** show that there is a similar chemical dependence of the tetragonal distortion parameter derived from optical absorption spectroscopy and from EPR.

The anisotropy of the *g*-factor Δg ($\Delta g = g_{//} - g_{\perp}$), is also related to Cu^{2+} site distortion. Δg is lower in alkali-rich than in alkali-poor borate glasses (**Fig. 7b**), an indication of a more symmetrical site. This is in line with the conclusion drawn above from the values of the *g* and *A* EPR parameters. They indicate that larger bond lengths occur in alkali-poor borate glasses, which show EPR parameters similar to the values found in aqua- complexes. The Cu^{2+} site distortion may be also qualitatively estimated by a tetragonal distortion parameter defined by the $g_{//}/A_{//}$ ratio (in cm values) [41] and shown on (**Fig. 11b**): planar complexes give rise to values in the range 110-120 cm and an increasing tetragonal distortion corresponds to values in the range 130–150 cm and 180–250 cm from a slight to a strong distortion. In alkali borate glasses, we find a ratio between 150 and 200 cm. The lower values of this parameter with increasing alkali content confirm that the distortion of the Cu^{2+} site progressively decreases at high alkali content.

Complementary evidence for an increasing distortion of the Cu^{2+} site at high alkali content is provided by the large values of the *Dt* tetragonal field parameter (**Fig. 11a**) and by the broadening of the Cu^{2+} absorption band with at high alkali content (**Fig. 4**). These variations result from an increasing splitting of the Gaussian components evidenced by the band fitting (**Table S1**).

4.5 The Cu-O bonding

The parameters of the in-plane σ- and π-bonding between the Cu^{2+} *d*- orbitals and the ligand *p*-orbitals can be assessed by the parameters α^2 and β_1^2 that represent the contribution of the *3d* atomic orbitals of the cupric ion to the $^2B_{1g}$ and $^2B_{2g}$ anti bonding orbitals, respectively. The former measures the in-plane σ-bonding coefficient between the $d_{x^2-y^2}$ orbital of Cu^{2+} and the ligand *2p* orbital ($^2B_{1g}$ level). The latter describes the in-plane π-antibonding between the $3d_{xy}$ orbital of Cu^{2+} and the *2p*-orbitals of the ligand ($^2B_{2g}$ level). α^2 and β_1^2 are defined by the following relations [29,30,49,50]:

$$\alpha^2 = \frac{7}{4}\left[\frac{|A_{//}|}{P} - \frac{|A|}{P} + \frac{2}{3}g_{//} - \frac{5}{21}g_{\perp} - \frac{6}{7}\right] \quad (5)$$

$$\beta_1^2 = \frac{E(\nu_2)}{4\lambda\alpha^2}\left[1 - \frac{g_{//}}{g_{\perp}}\right] \quad (6)$$

where *P* is the dipolar hyperfine coupling parameter, $0.036 cm^{-1}$, $A=[(1/3)A_{||}+(2/3)A_{\perp}]$ and λ is the spin-orbit coupling constant ($-828\ cm^{-1}$). $E(\nu_2)$ represents the energy of the ν_2 ($B_{1g} \rightarrow B_{2g}$) transition, as defined on **Fig. 10**. The fit of the broad Cu^{2+} absorption band gives a more reliable value of the energy of this electronic transition than the position of its apparent maximum, improving the evaluation of normalized covalency values. The α^2 and β_1^2 coefficients are indicators of the bonding character, with values between 0.5 and 1 (**Table S4**). A value of 1 indicates a purely ionic bond. If the overlapping integral is vanishingly small and $\alpha^2 = 0.5$, the covalency between the oxygen ligand orbitals and the d_{xy} orbital is high. The values of α^2 and β_1^2 are close to those found in the literature for borate glasses covering a large set of compositions [12,13,38,41,50]. These parameters retain an intermediate value, showing that both the in-plane *σ*-bonding and the in-plane-*π*-bonding between Cu^{2+} and O neighbors are moderately covalent. The values of α^2

remain close to around 0.8 in the borate glasses investigated. By contrast, the β_1^2 parameter decreases at higher alkali content and lower cationic field strength, from Li- to Na- and K borate glasses (**Fig. 12**). This indicates a more covalent character of the Cu^{2+}-O π-bonds, resulting from the weakening of the B-O bonds due to the progressive conversion of $^{[3]}B$ into $^{[4]}B$ with increasing alkali concentration. This is consistent with an increased electron delocalization in alkali-rich compositions shown by EPR (see **4.1**).

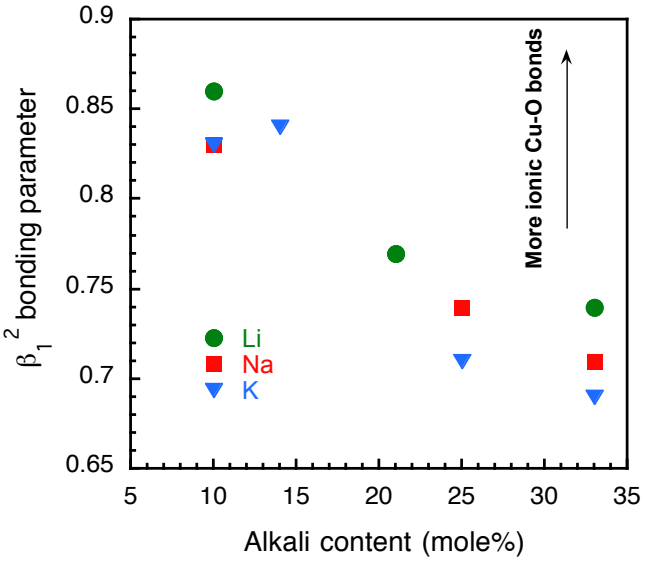

Fig. 12. Chemical dependence of the bonding coefficient (in-plane π-bonding)

4.6 Cu^{2+} speciation in alkali borate glasses

The chemical dependence of the spectroscopic properties of Cu^{2+} in alkali borate glasses is different from that observed for other divalent transition elements, as Co^{2+} or Ni^{2+}. Indeed, these elements suffer a dramatic coordination change from 4- and/or 5-coordination in high or medium alkali borate glasses to 6-coordination at low alkali content [7,8,32,33]. This coordination change was rationalized by Wong and Angell [5] as resulting from the competition, in highly acid oxide glasses such as B_2O_3, between network formers such as B or Si and intermediate cations as transition elements for available oxygen ligands. By contrast, there is no coordination change of Cu^{2+} in alkali borate glasses. Instead, the distortion of the elongated Cu^{2+} octahedral sites varies as a function of glass composition. The equatorial and axial ligands of the Cu-site play a distinct role, the former being more strongly bound to Cu^{2+} than the latter. This

414 is illustrated by the structure of CuO, that is not a face-centered cubic (fcc) arrangement, as Cu^{2+} ions are only
415 coordinated by four oxygen atoms, the two axial oxygen neighbors being in a remote position [51].
416 The detailed picture of the speciation of Cu^{2+} in alkali borate glasses brought by combining optical absorption
417 and EPR data is consistent with these expectations, demonstrating an important compositional dependence of several
418 key structural parameters. The Cu^{2+} sites are more distorted in alkali-poor than in alkali-rich compositions, as discussed
419 in **§4.4**. The topology of these sites is also less distributed than in alkali rich glasses where disorder effects cause a
420 broadening of Cu^{2+} optical absorption and EPR spectral features: in these compositions, the formation of $^{[4]}B$ provides
421 an increased diversity of borate supergroups [2] that leads to a broader distribution of Cu-site geometry. The medium
422 range order around Cu^{2+} obeys Pauling rules, as a consequence of the need for charge neutrality: $^{[3]}B$ and $^{[4]}B$ share 1
423 and 0.75 v.u. charges with their O-ligands, respectively, which will modify the Cu-site geometry. This diversity of
424 medium range organization is well illustrated by the crystal chemistry of crystalline Cu-borates [52-55] (**Fig. S4**). The
425 absence of clustering of Cu^{2+} ions in low-alkali borate glasses is demonstrated by the absence of superparamagnetic
426 contributions and of EPR signal broadening. It is probably one of the most original properties of these glasses. It is at
427 variance to what is observed for other divalent transition elements Co^{2+} and Ni^{2+} and for Zn^{2+} in the same glass
428 compositions [8,9,32,33].
429
430 ***4.7 Molecular scale scenarios using bond-valence approach***
431 Bond-valence requirements [56,57] constrain the role of borate groups due to the existence of two B
432 coordination numbers. A preferential bonding of Cu^{2+} sites to either BO_3 triangles or BO_4 tetrahedra may be
433 rationalized by considering bond-valence constraints: trigonal B brings a charge compensation of 1 valence unit (v.u.)
434 to its oxygen ligands, as compared to 0.75 v.u. for tetrahedral B (**Fig. 13a**). This increases the charge deficit of the
435 oxygen involved in bonding to a tetrahedral vs. a triangular boron. There is no strong bonding possible between a $^{[3]}B$-
436 $^{[3]}B$ bridging oxygen and Cu^{2+} sites, the charge of this oxygen being already neutralized by the two $^{[3]}B$-O bonds. This
437 bonding requirement explains the contrast in the reactivity of borate melts for dissolving metals: it is noteworthy that
438 molten B_2O_3 dissolves about 40 times less Cu^{2+} than molten alkali borate melts [58]. Such a difference may be related
439 to the different coordination state of B between these two melts, $^{[3]}B$ in the former and $^{[4]}B$ in the latter.
440 A simple scenario occurs for a $^{[3]}B$ linked to two Cu-sites (**Fig. 13d**), as the shared oxygen atoms receive 1 v.u.
441 from B and twice 0.5 v.u. from the Cu^{2+} sites, ensuring their neutrality. Similarly, when an equatorial ligand serves as a

bridging oxygen $^{[4]}$B-O-$^{[4]}$B (**Fig. 13b**), its charge is compensated. As a consequence, the axial ligands are found in a remote position, as observed in crystalline alkali-copper borates (see **Fig. S4**), which avoids Cu^{2+} overbonding.

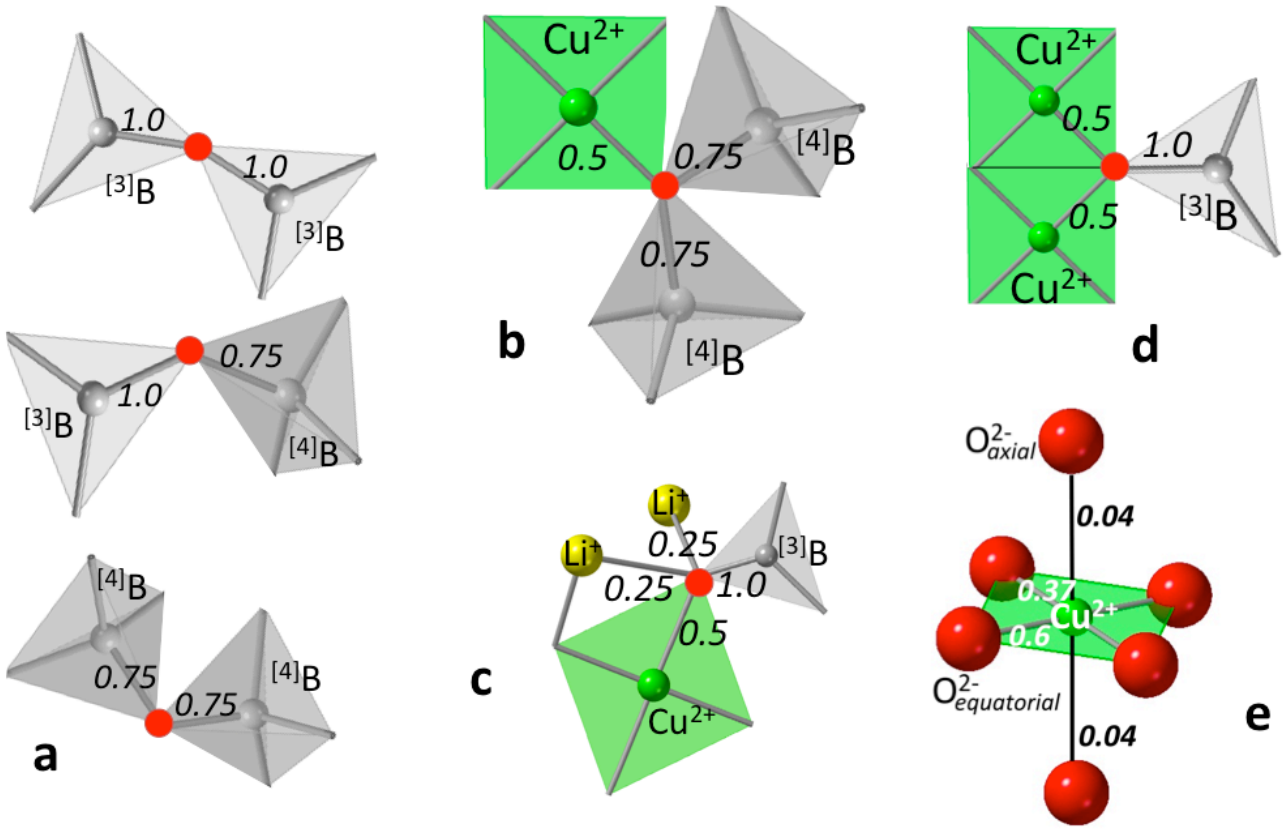

Fig. 13. Structural order predicted from a bond-valence modeling. (a): the charge received by the bridging oxygen from its B-neighbors is deduced from the existing bonds, decreasing from 2.0 v.u. to 1.75 v.u. and 1.5 v.u. from the top to the bottom, as B coordination increases. (b) and (d) illustrate how oxygen atoms bridge Cu-sites and the borate framework. (c): Local structure of HT α-$Li_6CuB_4O_{10}$, showing the charge compensating role played by Li^+ ions. (e): weak contribution of the axial ligands in HT α-$Li_6CuB_4O_{10}$ using calculations from Relation 9.

Alkalis help adjust the bond-valence requirements for oxygen atoms: in the scenario presented on **Fig. 13c**, the oxygen atom receives 1.5 v.u. from bridging to Cu^{2+} and $^{[3]}B$ and it receives an additional twice 0.25 v.u. charge compensation from the two Li^+ neighbors.. The coordination number of the alkali plays an important role in the contribution of alkalis: as Li^+ is tetrahedrally coordinated in α-$Li_6CuB_4O_{10}$, and Na^+ is 7-coordinated in $Na_2Cu_2B_{12}O_{21}$, Li^+ and Na^+ contribute 0.25 and 0.14 v.u., respectively. However, the size of the alkali does not modify the coordination number of Cu^{2+}, which remains located in distorted octahedron geometry. As a consequence, the short-range order in glasses does not correspond to a substitution mechanism (e.g. $Cu^{2+} \rightarrow Li^+$ (K^+) evocated in borate glasses [59]. The coordination change observed in Li-, Na- or K- oxide glasses containing Co^{2+} or Ni^{2+} [7-9] does not correspond to such substitution schemes. Tetrahedrally coordinated transition elements in high K-glasses correspond to a network-forming position of Ni and Co, i.e. tetrahedral sites that are corner-linked to the glass framework. By contrast, bond-valence requirements impose higher coordination numbers of these transition elements in Li-glasses, the reverse to what would be expected by considering the size of the alkali.

The bond-valence model provides a way to evaluate the relative charge s_{ij} of the equatorial and axial Cu^{2+} ligands as a function of the length of the bond R_{ij} [56,57]:

$$s_{ij} = \exp\left(\frac{R_O - R_{ij}}{B}\right) \quad (9)$$

where R_0 and B are the bond-valence parameters of the ion pair *ij*, empirically defined as 1.67Å and 0.37Å, respectively, for Cu^{2+} [57]. The application to the speciation of Cu^{2+} in borates is illustrated in **Fig. 13e**. In the high temperature polymorph of α-$Li_6CuB_4O_{10}$, the Cu-$O_{equatorial}$ distances are 1.86 and 2.03Å, as the Cu-O_{axial} distance is 2.82Å. The predicted bond-valence values are 0.6, 0.37 and 0.04 v.u., respectively. This demonstrates that, although minute modifications of the Cu-O_{axial} distances modify the spectroscopic properties of Cu^{2+}, the structural importance of such changes is limited in terms of electrical neutrality of the local structure. A nice demonstration of this sensitivity has been shown by co-doping experiments of sodium borate glasses with high field strength cations [14,18]. In that case, even low concentrations of additional cations modify the EPR signature of Cu^{2+} in these glasses. This is a consequence of the competition for charge compensation observed in multicomponent glasses: a high field strength cation as Zr^{4+} occurs in alkali-containing glasses as an octahedral species, which requires charge-compensating alkalis [60]. As underlined in other glass systems [60,61], the competition between various structural environments of cations is at the origin of the modification of glass properties, an illustration of the structure-property relationships in glasses.

Such a competition for charge-compensation between network forming (e.g. B^{3+}) and networking elements (e.g. Zr^{4+}) has been observed in Na-Ca alumino-borosilicate glasses with a decreasing preference in the order: Al> Zr> Zn>B [62]. It is interesting that the codoping experiments on sodium borate glasses [14,18] confirm that Zr competes favorably with B for charge compensation, forming $^{[3]}$B at the expense of $^{[4]}$B and accordingly modifying the local structure around Cu^{2+}.

These molecular-scale considerations predict that the effective charge of the axial ligands of Cu^{2+} increases with the alkali content of the glass, as they are more loosely attached to Cu^{2+} than the equatorial ones. The three scenarios depicted in **Fig. 13a** show that the charge deficit of a bridging oxygen decreases with the coordination state of its B neighbors, corresponding to the evolution expected for the B coordination number with decreasing alkali content in binary borate glasses. At low alkali levels, a lower effective charge of axial Cu^{2+} ligands leads to an increase of the Cu-O bond length, resulting in a higher site distortion. As the planar $^{[3]}$B sites favor rigid, 2D-based, polymeric supergroups [1,2], the local disorder is also expected to decrease at the same time.

5. CONCLUSION

R_2O-B_2O_3 glasses containing 0.2 mol% CuO exhibit a cyan to blue color change as a function of the alkali content. These glasses were investigated using UV–vis-near IR absorption spectra and EPR spectroscopy. Optical absorption spectra show an asymmetric absorption band corresponding to three transitions of Cu^{2+} ions from the $^2B_{1g}(d_{x^2-y^2})$ ground level to the partially empty $^2A_{1g}(d_{z^2})$, $^2B_{2g}(d_{xy})$ and $^2E_g(d_{xz}, d_{yz})$ levels, consistent with distorted Cu2+ octahedral sites. The correlation between the data obtained from EPR, as the anisotropy of the *g*-factor and the tetragonal distortion parameter- and from Cu^{2+} optical spectroscopy, as the tetragonal field parameter *Dt* and the splitting of the Gaussian components, shows that the Cu^{2+} sites are more distorted in alkali-poor than in alkali-rich compositions. Low-alkali glasses show a noteworthy similarity with the spectroscopic parameters of aqueous Cu^{2+} complexes. These structural modifications are linked to a more covalent character of the Cu^{2+}-O π-bonds, resulting from the weakening of the B-O bonds due to the progressive conversion of $^{[3]}$B into $^{[4]}$B with increasing alkali concentration. The Cu^{2+} sites are also more distributed in alkali rich glasses where the formation of $^{[4]}$B provides a larger distribution of the geometry of borate supergroups that leads to a broader distribution of the geometry of Cu-sites.

The originality of the spectroscopic properties of Cu^{2+} as compared to Ni^{2+} or Co^{2+} in alkali borate glasses comes from several factors. For most spectroscopic parameters, the pertinent parameter is not the cation field strength but the cation concentration. The cation clustering observed for Co^{2+} and Ni^{2+} in low-alkali borate glasses is not observed for Cu^{2+}. In contrast to borate glasses containing Co^{2+} or Ni^{2+}, there is no coordination change as a function of glass composition, tetrahedral Cu^{2+} being rather seldom in oxide-based materials [52]. Instead of major changes of Cu^{2+} coordination , the spectroscopic properties show a modification of the axial elongation of the Cu^{2+} octahedral site with glass composition. This may result from the modification of the Jahn Teller effect by the local constraints due to glass structure, in particular in presence of rigid super-structural borate units in the alkali-poor compositions.

Bond-valence considerations predict that the effective charge of the axial ligands of Cu^{2+} increases with the alkali content of the glass, affecting primarily the distortion of the Cu^{2+} site. The three scenarios depicted in **Fig. 13a** show that the charge deficit of a bridging oxygen decreases with B coordination, as the bond-valence of the B-O bond increases from 0.75 to 1 v.u. This causes a deficit of this bridging oxygen of 0.5, 0.25 and 0 v.u. for the $^{[4]}$B -O-$^{[4]}$B, $^{[4]}$B-O-$^{[3]}$B and $^{[3]}$B-O-$^{[3]}$B linkages, respectively, corresponding to the evolution expected for the B coordination number with decreasing alkali content in binary borate glasses. The charge deficit of the $^{[4]}$B-O-$^{[4]}$B bridging oxygen explains the $^{[4]}$B maximum observed in alkali borate systems. As early as in 1952, Abe postulated that adjacent tetrahedral boron atoms are energetically unfavorable [64], because of the difficulty for large alkalis to fit in the glassy framework for achieving charge compensation around this bridging oxygen.

These observations illustrate the usefulness of Cu^{2+} as a sensitive structural probe [63]. The coordination change usually observed for transition elements in alkali borate glasses is replaced by a modification of the distortion of the Cu^{2+} octahedral site This original property gives rise to more subtle color changes in the absence of drastic coordination changes.

DECLARATION OF COMPETING INTEREST

The authors declare that they have no known competing financial interests or personal relationships that could have appeared to influence the work reported in this paper.

References

1. A.C. Wright, My borate life: an enigmatic journey, Int. J. Appl. Glass Sci. 6 (2015) 45-63.
2. A.C. Wright, N.M. Vedishcheva, Borate networks: rigidity versus dimensionality, Phys. Chem. Glasses 57 (2016) 1-14.
3. J. Wu, J.F. Stebbins, T. Rouxel, Cation field strength effects on boron coordination in binary borate glasses, J. Am. Ceram. Soc. 97 (2014) 2794-2801.
4. W.A. Weyl, Coloured Glasses. Society of Glass Technology, 1951.
5. J. Wong , C.A. Angell, Glass structure by spectroscopy. M. Dekker, New York, 1976.
6. L. Galoisy, G. Calas, Spectroscopic evidence of five-coordinated Ni in $CaNiSi_2O_6$ glass. Amer. Mineral. 76 (1991) 1777-1780.
7. L. Galoisy, G. Calas, L. Cormier, B. Marcq, M.H. Thibault, Overview of the environment of Ni in oxide glasses in relation to the glass colouration, Phys. Chem. Glasses 46 (2005) 394–399.
8. L. Galoisy, G. Calas, Role of alkali field strength on the speciation of Ni^{2+} in alkali borate glasses: comparison with crystalline Ni-borates, J. Non-Cryst. Solids 577 (2022) 121320.
9. M.O.J.Y. Hunault, L. Galoisy, G. Lelong, M. Newville, G. Calas, Effect of cation field strength on Co^{2+} speciation in alkali-borate glasses, J. Non-Cryst. Solids 451 (2016) 101–110.
10. M.O.J.Y. Hunault, G. Lelong, L. Cormier, L. Galoisy, P.L. Solari, G. Calas, Speciation change of uranyl in lithium borate glasses, Inorg. Chem. 58 (2019) 6858-6865.
11. R.G. Burns, Mineralogical applications of crystal field theory. Cambridge Univ. Press, Cambridge, 1993.
12. H. Kawazoe, H. Hosono, T. Kanazawa, Electronic structure and properties of oxide glasses (II) Basicity measured by copper (II) ion probe in Na_2O-P_2O_5, K_2O-B_2O_3 and K_2SO_4-$ZnSO_4$ glasses, J. Non-Cryst. Solids 29 (1978) 173-186.
13. H. Hosono, H. Kawazoe, T. Kanazawa, ESR and optical absorption of cupric ion in borate glasses, J. Non-Cryst. Solids 34 (1979) 339-356.
14. F. Funabiki, S. Matsuishi, H. Hosono, Ligand field modification around Cu^{2+} ions in sodium borate glass by codoping, J. Phys. Chem. A 115 (2011) 5081-5088.
15. M.O.J.Y. Hunault, C. Loisel, Looking through model medieval green glasses: From color to recipe, Int. J. Appl. Glass Sci. 11 (2020) 463-470.
16. N. Capobianco, M.O.J.Y. Hunault, S. Balcon-Berry, L. Galoisy, D. Sandron, G. Calas, The Grande Rose of the Reims Cathedral: an eight-century perspective on the colour management of medieval stained glass, Sci. Rep. 9 (2019) 3287.
17. A.Silvestri, S. Tonietto, F. D'Acapito, G. Molin, The role of copper on colour of palaeo-Christian glass mosaic tesserae : An XAS study, J. Cult. Herit. 13 (2012) 137–144.
18. F. Funabiki, S. Matsuishi, H. Hosono, Elucidation of codoping effect in Cu^{2+} containing sodium borate glass, J. Non-Cryst. Solids, 358 (2012) 2446-2449.
19. C.C. Ding, S.Y. Wu, M.Q. Kuang, X.F. Hu, G.L. Li, Studies of the local distortions and the EPR parameters for Cu^{2+} in xLi_2O-(30-x)Na_2O-69.5B_2O glasses, Z. Naturforsch. A71 (2016) 249-254.

20. H.M. Zhang, X. Wan, Theoretical studies of spin Hamiltonian parameters for the tetragonally elongated Cu^{2+} centers in $ARbB_4O_7$ (A = Li, Na, K) glasses, J. Non-Cryst. Solids 361 (2013) 43-46.
21. W.H. Wei, C.J. Hou, M. Lu, W.Q. Liu, Spin-Hamiltonian parameters and defect structure of the copper (2+) center in lithium borate, Spectrosc. Lett. 46 (2013) 297-300.
22. H. Imagawa, ESR Studies of cupric ion in various oxide glasses. Phys. Stat. Solidi 30 (1968) 469-478.
23. Q. Xu, T. Maekawa, K. Kawamura, T. Yokokawa, Exafs and Xanes investigations of sodium-borate glasses containing copper ions, Phys. Chem. Glasses 31(1990) 10–18.
24. S. Gomez-Salces, F. Aguado, R. Valiente, F. Rodrigues, Unraveling the coordination geometry of copper(II) ions in aqueous solution through absorption intensity. Angew. Chem. Int. Ed. 51 (2012) 9335-9338.
25. Z.Y. Yao, D. Möncke, E.I. Kamitsos, P. Houizot, F. Célarié, T. Rouxel, L. Wondraczek, Structure and mechanical properties of copper–lead and copper–zinc borate glasses, J. Non-Cryst. Solids 435 (2016) 55-68.
26. S. Gomez, I. Urra, R. Valiente, F. Rodriguez, Spectroscopic study of Cu^{2+} and Cu^{+} ions in high-transmission glass. Electronic structure and Cu^{2+}/Cu^{+} concentrations, J. Phys.: Condens. Matter 22 (2010) 295505.
27. S.R. Qiu, B.C. Wood, P.R. Ehrmann, S.G. Demos, P.E. Miller, K.I. Schaffers, T.I. Suratwala, R.K. Brow, Origins of optical absorption characteristics of Cu^{2+} complexes in aqueous solutions, Phys. Chem. Chem. Phys. 17 (2015) 18913–18923.
28. A. Godiksen, P.N.R. Vennestrøm, S.B. Rasmussen, S. Mossin, Identification and quantification of copper sites in zeolites by electron paramagnetic resonance spectroscopy, Top. Catal. 60 (2017) 13-29.
29. R. P. S. Chakradhar, K. P. Ramesh, J. L. Rao, J. Ramakrishna, Mixed alkali effect in borate glasses - electron paramagnetic resonance and optical absorption studies in Cu^{2+} doped $xNa_2O–(30-x)K_2O–70B_2O_3$ glasses, J. Phys.: Condens. Matter 15 (2003) 1469-1486.
30. R.P.S. Chakradhar, B. Yasoda, J. Lakshmana Rao, N.O. Gopal, Mixed alkali effect in $Li_2O–Na_2O–B_2O_3$ glasses containing CuO – An EPR and optical study, J. Non-Cryst. Solids 352 (2006) 3864–3871.
31. A.R. Babu, S. Yusub, V. Aruna, N.S.Ram, P.M. Vinaya Teja, Y. Chaitanya, The influence of Cu^{2+} ions on the ionic, electronic conductivity and optical characteristics of Li_2O-SrO-B_2O_3 system, J. Non-Cryst. Solids 575 (2022) 121210.
32. L. Cormier, L. Galoisy, G. Calas, Evidence of Ni-containing ordered domains in low-alkali borate glasses. Europhys. Lett. 45 (1999) 572-578.
33. L. Galoisy, L. Cormier, G. Calas, V. Briois, Environment of Ni, Co and Zn in low alkali borate glasses: information from EXAFS and XANES spectra, J. Non-Cryst. Solids 293-295 (2001) 105-111.
34. G. Giugliarelli, S. Cannistraro, Simulation of EPR spectra of Cu^{2+} complexes with statistical distribution of the g-factor and hyperfine splitting, Chem. Phys. 98 (1985) 115–122.
35. W.B. Lewis, M. Alei, L.O. Morgan, Magnetic resonance studies on copper(II) complex ions in solution. I. Temperature dependences of the ^{17}O NMR and copper(II) EPR linewidths of $Cu(H_2O)_6$, J. Chem. Phys. 44 (1966) 2409-2417.
36. K.J. de Almeida, Z. Rinkevicius, H.W. Hugosson, A.C. Ferreira, H. Ågren, Modeling of EPR parameters of copper(II) aqua complexes, Chem. Phys. 332 (2007) 176-187.

37. L.D. Bogomolova, V.A. Zhachkin, T.K. Pavlushkina, (2015) Use of electron paramagnetic resonance for investigating glasses and raw materials, Glass Ceram. 72:117–122.
38. H. Kawazoe, H. Hosono, H. Kokumai, J. Nishii, T. Kanazawa, Structural distribution and rigidity of the glass network determined by EPR of Cu^{2+}, J. Non-Cryst.Solids 40 (1980) 291- 303.
39. J. Peisach, W.E. Blumberg, Structural implications derived from the analysis of electron paramagnetic resonance spectra of natural and artificial copper proteins, Arch. Biochem. Biophys. 165 (1974) 691-708.
40. W.M. Ames, S.C. Larsen, Density functional theory investigation of EPR parameters for tetragonal Cu(II) model complexes with oxygen ligands, J. Phys. Chem. A 113 (2009) 4305-4312.
41. T.H. Noh, E.L. Shim, Study of CuO content on physical and structural properties of Li_2O-B_2O_3-CuO glasses using electron paramagnetic resonance, J. Non-Cryst. Solids 474 (2017) 37-42.
42. A. Duran, J. M. F. Navarro, The colouring of glass by Cu^{2+} ions. Phys. Chem. Glasses, 26 (1985) 125–131.
43. A.B.P. Lever (1984) Inorganic electronic spectroscopy, 2nd edn. Elsevier, Amsterdam.
44. Q.H. Le, C. Friebe, W.C. Wang, L. Wondraczek, Spectroscopic properties of Cu^{2+} in alkaline earth metaphosphate, fluoride-phosphate and fluoride-phosphate-sulfate glasses, J. Non-Cryst. Solids X 4 (2019) 100037.
45. R.V. Pisarev, A.M. Kalashnikova, O. Schops, L.N. Bezmaternykh, Electronic transitions and genuine crystal-field parameters in copper metaborate CuB_2O_4, Phys. Rev. B 84 (2011) 075160.
46. A.D. Molchanova, M.A. Prosnikov, R.M. Dubrovin, V.Y. Davydov, R.V. Pisarev, K.N. Boldyrev, M.N. Popov, Lattice dynamics and electronic transitions in a structurally-complex layered copper borate $Cu_3(BO_3)_2$, Phys. Rev. B 96 (2017) 174305.
47. M. Wildner, G. Giester, M. Kersten, K. Langer, Polarized electronic absorption spectra of colourless chalcocyanite, $CuSO_4$, with a survey on crystal fields in Cu^{2+} minerals, Phys. Chem. Miner. 41 (2014) 669-680.
48. E. König, E. S. Kremer, (1977) Ligand field energy diagrams. Springer US, Boston, MA.
49. H.A. Kuska, M.T. Rogers, R.E. Drullinger, Effect of substituents on the anisotropic electron spin resonance parameters in copper acetylacetones, J. Phys. Chem. 71 (1967) 109-114.
50. A. Bhogi, R.V. Kumar, P. Kistaiah, Effect of alkaline earths on spectroscopic and structural properties of Cu^{2+} ions-doped lithium borate glasses, J. Non-Cryst. Solids 426 (2015) 47-54.
51. S. Asbrink, A. Waskowska, CuO: X-ray single-crystal structure determination at 196 K and room temperature, J. Phys. Condens. Matter 3 (1991) 8173.
52. M. Martinez-Ripoll, S. Martinez-Carrera, S. GarciaBlanco, The crystal structure of copper metaborate CuB_2O_4 Acta Cryst.. B 27 (1971) 677-681.
53. O.C. Gagné, F.C. Hawthorne, Bond-length distributions for ions bonded to oxygen: results for the transition metals and quantification of the factors underlying bond-length variation in inorganic solids, IUCrJ 7 (2020) 581-629.
54. F. Rajah, M. Graia, T. Mhiri, Synthesis and single crystal X-ray structure of the monoclinic sodium copper borate ($Na_2Cu_2B_{12}O_{21}$) Chem. Sci. Trans. 1 (2012) 103-110.

55. F. Strauss, G. Rousse, D.A.D. Corte, C. Giacobbe, R. Dominko, Impact of structural polymorphism on ionic conductivity in lithium copper pyroborate $Li_6CuB_4O_{10}$, Inorg. Chem. 57 (2018) 11646-11654.
56. N.E. Brese, M. O'Keefe, Bond-valence parameters for solids**,** Acta Cryst. B 47 (1991) 192-197.
57. I.D. Brown, D. Altermatt, Bond-valence parameters obtained from a systematic analysis of the inorganic crystal structure database, Acta Cryst. B 41 (1985) 244-247.
58. T. Amietszajew, S. Seetharaman, R. Bhagat, The solubility of specific metal oxides in molten borate glass, J. Am. Ceram. Soc. 98 (2015) 2984-2987.
59. B. Padlyak, W.R. Romanowski, R. Lisiecki, O. Smyrnov, A. Drzewiecki, Ya. Burak, V. Adamiv, I. Teslyuk, Synthesis and spectroscopy of tetraborate glasses doped with copper, J. Non-Cryst. Solids 356 (2010) 2033-2037.
60. L. Galoisy, E. Pélegrin, M. A. Arrio, P. Ildefonse, G. Calas, D. Ghaleb, C. Fillet, F. Pacaud, Evidence for 6-coordinated zirconium in inactive nuclear waste glasses, J. Am. Ceram. Soc. 82 (1999) 2219-2224.
61. G. Calas, L. Galoisy, L. Cormier, G. Ferlat, G. Lelong, The structural properties of cations in nuclear glasses, Proc. Mater. Sci. 7 (2014) 23-31.
62. L. Cormier, D. Ghaleb, J.M. Delaye, G. Calas, Competition for charge compensation in borosilicate glasses: wide-angle X-ray scattering and molecular dynamics calculations, Phys. Rev. B 61 (2000) 14495-14499.
63. K.J. de Almeida, N.A. Murugan, Z. Rinkevicius, H.W. Hugosson, O. Vahtras, H. Agren, A. Cesar, Conformations, structural transitions and visible near-infrared absorption spectra of four-, five- and six-coordinated Cu(II) aqua complexes, Phys. Chem. Chem. Phys. 11 (2009) 508-519.
64. T. Abe, Borosilicate glasses, J. Am. Ceram. Soc. 35 (1952) 284-299.